Wide Wavelength Photon Harvesting in Dye-Sensitized Solar Cells utilizing Cobalt Complex Redox Electrolyte: Implication of Surface Passivation

Anusha Pradhan*, Maryala Sai Kiran, Gaurav Kapil, Shuzi Hayase, Shyam S. Pandey*

Graduate School of Life Science and Systems Engineering, Kyushu Institute of Technology, 2-4, Hibikino, Wakamatsu, Kitakyushu 808-0196, Japan

E-mail address: shyam@life.kyutech.ac.jp

ABSTRACT

A combination of near infra-red (NIR) photon harvesting and cobalt electrolytes having deeper redox energy level are needed for the fabrication of high efficiency dye-sensitized solar cells (DSSCs). A logical molecular design of unsymmetrical squaraine dye (SQ-110) as a representative of NIR dyes has been demonstrated to function well in DSSC using cobalt complex redox electrolyte. Problem of mass transport limitations due to the bulky cobalt complex ions leading to relatively enhanced charge recombination was amicably solved by single as well as multiple compact metal oxide surface passivation on both of the transparent conducting oxide substrate as well as mesoporous TiO_2. Complete absence of light absorption beyond 550 nm wavelength region by D-35 and utilization of a complementary light harvesting dye SQ-110 led to efficient wide wavelength photon harvesting. DSSC fabricated using a dye cocktail of D-35 and SQ-110 in 4:1 ratio resulted in to photoconversion efficiency (PCE) of 7.2 %, which is much higher as compared to the constituent individual sensitizers D-35 (3.6 %) and SQ-110 (1.9 %). This synergistic enhancement in PCE by dye cocktail was associated with the mutual co-operation of respective dyes in terms controlling the dye aggregation and complementary photon harvesting. In this this dye cocktail system, D-35 is involved in the prevention of dye aggregation, lower wavelength photon harvesting and energy transfer induced photocurrent enhancement.

Keywords: Photosensitization, Dye-sensitized solar cells, Squaraine dyes, Cobalt electrolyte, Surface Passivation, Energy transfer, FRET

1. Introduction

Solar cells have attracted huge attentions towards the quest for harnessing immense solar energy since it converts solar energy directly into most conveniently usable electrical energy [1]. This led to the emergence of already commercialized solar cells based on silicon, GaAs, CIGS, CdTe etc. [2-4]. High cost of production of these solar cells is still one of bottlenecks for their large-scale implementation at common mass level. To circumvent this issue, research interest towards next generation solar cells like, thin film polymer solar cells, dye-sensitized solar cell (DSSCs) and recently entered perovskite solar cells got momentum [5]. Therefore, in the world of acute need for the renewable energy, DSSCs have emerged as one of the promising candidates owing to its environment friendly production, low raw materials cost and ease of fabrication [6]. Since the report of appreciably good photoconversion efficiency (PCE) over 7 % in 1991, past two decades have seen tremendous growth of research interests in DSSCs pertaining to the further enhancement in the PCE [7]. It is well known that the key elements for enhancing the PCE of a solar cell are the short-circuit current density (Jsc) and open-circuit voltage (Voc), where, Jsc is controlled by efficient and panchromatic photon harvesting while Voc is governed by the judicious selection of mesoporous semiconductor and redox electrolyte. Result of the amicable optimization of the DSSC components like conducting substrates, mesoporous wideband semiconductors, sensitizing dyes and counter electrode materials led to nearly quantitative photon harvesting in the visible wavelength region (400-700) with PCE over 12% [8]. Sensitizing dyes are one of crucial components of DSSC being light absorber and availability of good photon flux (>55 %) beyond visible region are needed to be harvested for enhancing the PCE further [9]. This urges for the urgent attention towards design and development of efficient near infra-red (NIR) dyes and their incorporation with efficient visible sensitizers in order to boost the PCE by wide wavelength photon harvesting and accelerate commercialization DSSCs.

In spite of the fact that Ruthenium complex based dyes have dominated their presence in terms of stability and good PCE but concerns about the cost and rarity of Ruthenium led to the emergence of metal free organic dyes [10]. Metal free organic dyes in general bear donor-π-bridge-acceptor (D-π-A) molecular framework allowing the smooth π-π^* electronic transition and offers the synthetic flexibility and versatility owing to a large variation of D and A moieties. To extend the optical absorption window in these dyes, electron acceptors like benzothiadiazole, benzotriazole, quinoxaline and diketopyrrolopyrrole etc. in the D-A-π-A framework have although attempted but their very high tendency for aggregation resulted into hampered PCE [11-14]. In order to have panchromatic photosensitization, mixing two or more dyes (dye-cocktail) with complementary light absorption have been widely utilized leading to enhanced PCE [15-16]. Electrolytes in DSSC are another most important component and control the overall PCE by controlling the Voc. Voc in DSSCs is governed by energy difference between the Fermi level of the wide band gap semiconductor and energy level of the redox electrolyte. Since the inception of DSSCs, iodine based redox electrolytes have been most widely utilized, but their corrosiveness, deep color and search for electrolytes with deeper redox potential geared the investigation for alternate redox electrolytes. Amongst various electrolytes attempted for DSSCs, redox electrolytes based on cobalt complexes has emerged as strong contender owing to their relatively deeper redox potential leading enhanced PCE especially by contributing to enhance the Voc [17]. Research on DSSCs utilizing cobalt-based electrolytes has witnessed that unlike iodine based redox electrolytes, success was limited to selected sensitizes owing to their relatively bulkier size causing slow ionic diffusion and enhanced charge recombination. Iodine electrolytes bearing negative charge are being repelled by negatively charged TiO_2 nanoparticles. On the other hand, positively charged cobalt complex exhibit attractive interaction leading to slow ion diffusion and enhanced charge recombination [18]. Therefore, TiO_2 surface should be effectively passivated either by utilizing sensitizing dyes with long alkyl chains to hinder the $Co^{3+/2+}$ reaching to uncovered TiO_2 surfaces along with post surface treatments of TiO_2 before dye adsorption [19]. Keeping this in

mind, TiO_2 surface treatment based on various metal oxides such as Al_2O_3, SiO_2, ZnO, MgO etc. has been used to form the compact metal oxide conformal layer in order to suppress the charge recombination due to back electron transfer [20-21].

Herein we would like to report the synthesis and characterization of a far-red sensitive Squaraine dye (SQ-110) as model of NIR dyes having intense light absorption mainly in the far-red region of the solar spectrum. Squaraine dyes exist in D-A-D Zwitter-ionic form using central squaric acid core as electron acceptor and logical utilization of various donor moieties provide the capability to tune the optical absorption window from visible the IR wavelength region [22]. In this work, SQ-110 has been designed logically with the primary requirement of introducing long alkyl chains necessary to work effectively with the bulky and positively charged $Co^{3+/2+}$ ions [23]. Since this sensitizing dye has a sharp and intense optical absorption only in the far-red wavelength region, another dye D-35 was used to make dye-cocktails in order to have photon harvesting in the wide wavelength region [24]. In an interesting report, Yan *et al* have also demonstrated the Cobalt electrolyte based DSSC employing dye cocktail of D35 and Dyenamo Blue where, there was about 16 % enhancement in the PCE for dye cocktail (8.7%) compared to Dynamo Blue (7.3 %) [25]. While in this work, there is a remarkable enhancement in the PCE from 3.6 % to 5.5 %, which was further improved to 7.2 % by surface passivation with compact metal oxide. Compact layer of different kind of metal oxides (single/multilayer) on both of the conducting substrate as well as mesoporous TiO_2 have also been conducted in order to investigate their implications on the suppression on charge recombination and photovoltaic performance. Squaraine dyes are prone dye aggregate formation needing auxiliary coadsorber like chenodeoxycholic acid (CDCA) to prevent dye aggregation and control the charge recombination. Interestingly, utilization of D-35 with SQ-110 in dye cocktail bypassed the use of the CDCA and serves the multiple roles of dye coadsorber, aggregation preventer and light harvester in lower wavelength region. Molecular structure of sensitizing dyes used for present investigation has been shown in the Fig. 1.

2. Experimental

2.1 Materials and methods

All of the chemicals for synthesis or solvents are of analytical/spectroscopic grade and used as received. Sensitizing dye D-35 was purchased from Dyenamo AB Company, Sweden. Synthesis of unsymmetrical squaraine dye (SQ-110) and its intermediates were confirmed by thin layer chromatography (TLC), high performance liquid chromatography (HPLC) for purity, matrix assisted laser desorption and ionization (MALDI)-time-of-flight (TOF)-mass and fast ion bombardment (FAB)-mass spectrometry for molecular mass. Nuclear magnetic resonance (NMR) (JEOL, 500 MHz) spectroscopic verification of structure was also conducted using Tetramethylsilane (TMS) as internal standard. Electronic absorption spectra in solution as well as thin film of dyes adsorbed on mesoporous TiO_2 were measured using UV–visible spectrophotometer (JASCO model V550). Fluorescence emission spectrum D-35 in ethanol solution was measured using fluorescence spectrometer (JASCO FP-6600) in order to study its spectral overlapping with the absorption spectrum of SQ-110. Fluorescence lifetimes for the dyes adsorbed on the thin film of ZrO_2 having thickness of about 4 μm were measured using a fluorescence lifetime measurement system (Quantarus Tau Model C-11370, Hamamatsu Photonics, Japan). Samples were excited by laser light source at wavelength of 470 nm and fluoresecence decay was measured at 680 nm for all the cases. Highest occupied molecular orbital (HOMO) energy level was estimated by photoelectron yield spectroscopy (Bunko Keiki, model KV-205 HK, Japan) while energy of lowest unoccupied molecular orbital (LUMO) was calculated by the relation LUMO = HOMO + Eg, where, Eg is the optical band gap. Eg was estimated from the onset of the optical absorption. Electrochemical impedance spectroscopy (EIS) was also used for characterizing the DSSCs using a frequency response analyzer (Solartron Analytical, 1255B), connected to a potentiostat (Solartron Analytical, 1287). An AC perturbation of 10 mV was applied in the frequency range from 5×10^{-3} to 10^5 Hz in similar environment condition to photovoltaic measurements.

2.1 Synthesis of SQ-110

Unsymmetrical squaraine dye (SQ-110) along with their intermediates were synthesized as per the scheme shown in Fig. 2. Starting indole derivatives 5-Methoxy-2,3,3-Trimethyl-Indole and 5-Carboxy-2,3,3-Trimetyl-Indole were synthesized following the method by Peng et al (26) and our earlier publication (27). Cobalt complexes like $[Co(bpy)_3(PF_6)_2]$ and $[Co(bpy)_3(PF_6)_3]$ used for the preparation of Cobalt based redox electrolyte were synthesized as per our earlier publication [28]

*2.1.1 Synthesis of 5-methoxy-2,3,3- trimethyl 3H-indole [**1**]*:

8.6 g (50 mmol) of 4-methoxy phenyl hydrazine hydrochloride, 10.9 g (125 mmol) of 3-methyl-2-Butanone and sodium acetate (4.0 g, 50 mmol) in 80 mL of Glacial acetic acid were taken in 300 ml round bottom flask and refluxed for 18 hours. Solvent was removed under reduced pressure and obtained compound was dissolved in chloroform followed by washing with water. Compound was concentrated and finally purified by flash column chromatography using Ethyl acetate and Hexane (1:1) as eluting solvent to obtain the 8.9 g of titled compound as brown viscous liquid in in 94% yield. HPLC purity (>98%), and MALDI-TOF mass (measured m/z: 248.0 $[M+2]^+$; calculated m/z: 246.19) confirms the synthesis of this intermediate.

*2.1.2 Synthesis of 5-Methoxy-2,3,3-Trimethyl-1-Dimethyl-Octyl-Indolium Iodide[**2**]*

In a round bottom flask, fitted with a condenser, 3.6 g (18.4 mmol) of compound (**1**) and 1.5 equivalents (7.4 gm; 27.6 mmol) of 3,7-Dimethyl-1-Octyl-Iodide were dissolved in 50 mL nitromethane and refluxed for 48 hours. After the completion of the reaction as confirmed by TLC, the solvent was evaporated completely and the compound was washed with ample diethyl ether to obtain the titled product as an orange viscous liquid in 67% yield and >98 % HPLC purity [FAB-MS Calculated, 330.28 and measured, 331.57 $(M+1)^+$].

*2.1.3 Synthesis of 5-Methoxy-2,3,3-Trimethyl-N-Dimethyl-octyl-Semisquaraine ethyl-ester[**3**]and its hydrolyzed product [**4**]*

4.6 g (10 mmol) of 5-Methoxy-2,3,3-Trimethyl-N-Dimethyl-Octyl-Indolium Iodide, 3mL (20 mmol) of 3,4-diethoxy-3-cyclobutene-1,2-dione, 1 mL of triethylamine (Et_3N) and 50 mL of ethanol were taken in a round bottom flask, refluxed and reaction progress was monitored by TLC and HPLC. Solvent was evaporated under reduced pressure and crude product was subjected to flash column chromatography using hexane/ethyl acetate to get the desired semisquaraine dye (**3**) in the 50% yield and 99 % purity [FAB-MS (calculated: 453.29) and measured (454.74)]. This semiquaraine dye (**3**) was subjected to the ester hydrolysis using NaOH in ethanol under reflux, which was finished in 30 min. Ethanol was removed, compound was neutralized with HCl and extracted with ethyl acetate and finally solvent was evaporated to get hydrolyzed semisquaraine dye (**4**) in quantitative yield as orange-yellow solid. [FAB-MS (calculated: 425.25) and measured (426.40)].

*2.1.4 Synthesis of 5-Carboxy-2,3,3-Trimethyl-Indole [**5**]*

7.5 g (49 mmol) of 4-Hydrazino benzoic acid was dissolved in 120 mL of glacial acetic acid. 6.8 g (78 mmol) of 3-Methyl-2-butanone and 8.3 g of sodium acetate were then added and reaction mixture was refluxed for 8 hours. Volume of the acetic acid was reduced to 25 % by evaporating under reduced pressure followed by addition of 9:1 water/methanol mixture. Solution was left for crystallization and finally filtered to get the product as light brown solid in 54% yield and >99 % purity as confirmed by HPLC and FAB-MS [(calculated: 203.24) and measured (204.0)].

*2.1.5 Synthesis of 5-Carboxy-2,3,3-Trimethyl-1-Dimethyl-OctylIndolium Iodide[**6**]*

In a round bottom flask fitted with a condenser, 2.0 g (9.6 mmol) of 5-Carboxy-2,3,3-trimethyl indole and 3.7 g (13.8 mmol) of 3,7-dimethyl-1-octyl iodide were dissolved in 40 mL acetonitrile and refluxed while monitoring the progress of the reaction by TLC. After completion of reaction in 48 hours,

solvent was removed at rotary evaporator and excess amount of ether was added for precipitation followed by filtration. Titled compound (**6**) was obtained as pinkish white solid in 60 % yield and 99 % purity. FAB-MS (calculated: 345.26) and (measured: 345.72) confirms the synthesis of intermediate.

2.1.6 Synthesis of squaraine dye SQ-110

In a round bottom flask fitted with condenser, 330 mg (0.7 mmol) of intermediate (**6**) and 300 mg (0.7 mmol) of the hydrolyzed semisquaraine dye (4) were dissolved in 50 ml of benzene-butanol (1:1) mixture, which was refluxed for 18 hours using Dean-Stark trap. After completion of the condensation, solvent was evaporated and the crude dye was purified by silica gel flash column chromatography using chloroform/methanol eluting solvent to get a dark blue solid in the 82% yield and >98 % purity as confirmed by HPLC. Finally, identity of the synthesized dye was confirmed by high resolution FAB-MS (calculated m/z: 750.4972; measured: 751.5012 $[M+1]^+$) and ^{1}H NMR (500 MHz, d6-DMSO): d/ppm = 7.95 (d, H-30), 7.92 (d, H-4), 7.34 (dd, H-6), 7.28 (d, H-27), 7.23 (dd, H-29), 6.95 (dd, H-7), 5.87 (s, H-10), 5.72 (s, H-23), 4.03 (t, 2H, H-13), 4.15 (t, 2H, H-35), 1.03 (s, 6H, H-11 & H-12), 1.13 (s, 6H, H-33 & H-34), 0.87 (m, 15H, H-20, H-21, H-22, H-42 & H-43).

2.2 Surface passivation with metal oxides

In this work, both of conducting fluorine-doped tin-oxide glass (FTO) as well as mesoporous TiO_2 were subjected to the metal oxide surface treatments. Various kind of compact metal oxide layers such as TiO_2, MgO, Al_2O_3 and Nb_2O_5 were formed in order to passivate the substrate surfaces using solution approach. FTO glass substrates were cut and sequentially washed with detergent, distilled water, acetone and isopropanol under sonication for 15 min. $TiCl_4$ surface treatment was conducted by dipping the substrates in 40 mM aqueous $TiCl_4$ solution at 70^{o}C for 30 min followed by sintering at 450^{o}C for 30 min to form very thin compact TiO_2 layer [29]. MgO and Al_2O_3 surface treatments were conducted following the protocol by Kakiage et al [30]. For the MgO surface treatment, substrates were dipped in the 50 mM

solution of magnesium ethoxide in ethanol at 25°C for 1 hour while for the Al_2O_3 surface treatment 25 mM of Aluminum isopropoxide in isopropanol at 25°C for 45 min. In both of the cases, surface treated substrates were finally baked at 500°C for 30 min. In the similar manner, Nb_2O_5 surface treatment was conducted using 20 mM solution Niobium-butoxide in isopropanol at 25°C for 30 min. followed by sintering of the substrates at 500°C for 30 min. Unlike compact TiO_2, MgO and Al_2O_3, which were conducted on mesoporous TiO_2, FTO surface treatment was only done by compact TiO_2 and Nb_2O_5 only.

2.3 Fabrication and characterization of dye-sensitized solar cells

DSSCs were fabricated using Ti-Nanoxide D/SP paste (Solaronix SA), which was coated on a FTO glass plate (Nippon Sheet Glass Co., Ltd.) by a doctor blading followed by baking at 450^0C for 30 min. This mesoporous TiO_2 layer having a thickness of about 6 μm was coated on FTO by screen printing. Mesoporous TiO_2 coated FTO substrates were then dipped in 0.2 mM ethanolic solution of respective dyes D-35, SQ-110 and their dye-cocktails at room temperature. Dye adsorption was conducted for a period 5 hours for the dye cocktails while it was 4 hours and 5 hours for the dyes SQ-110 and D-35, respectively. Counter electrode was prepared by the thermopyrolysis of spin-coated solution of H_2PtCl_6 in isopropanol on FTO. Photoanode and the counter electrodes were affixed using a 25 μm hot melt polymer film (Mitsui-DuPont Polychemicals Co., Ltd.) as spacer at 110°C. Electrolyte was injected through the small void created while placing the spacers and finally sealed with a UV curable resin. Cobalt electrolyte was comprised of 0.22M $[Co(bpy)_3(PF_6)_2]$, 0.033 M of $[Co(bpy)_3(PF_6)_2]$, 0.2 M of tert.-butyl-pyridine and 0.1 M $LiClO_4$ in acetonitrile. Photovoltaic performance was measured using a solar simulator (CEP-2000 Bunko Keiki Co. Ltd, Japan) equipped with a xenon lamp (Bunko Keiki BSO-X150LC) used as a source of simulated solar irradiation at 100 mW/cm^2, AM 1.5 G. Power of the light exposure was calibrated using an amorphous Si photodetector (Bunko Keiki BS-520 S/N 353). Photocurrent action spectra was also measured with a constant photon flux of 1×10^{16} photon/cm^2 in DC mode using the action spectrum measurement system connected to the solar simulator. The cell area was 0.25 cm^2, which was precisely defined using a black metal mask.

3. Results and Discussion

3.1 Optical characterization

Electronic absorption spectra of sensitizing dyes D-35 and SQ-110 in ethanol solution and thin films of dyes adsorbed on the mesoporous TiO_2 (3 μm) are depicted in the Fig. 3. It can be seen that D-35 in ethanol solution exhibits optical absorption maximum (λ_{max}) at 444 nm with a molar extinction coefficient (ε) of 2.57×10^4 $dm^3mol^{-1}cm^{-1}$, which is associated with the π-π* transition from the HOMO of the dye to its LUMO. Upon adsorption to TiO_2 surface, there is about 28 nm red shift in λ_{max} and spectral broadening, which is associated with the interaction of dye molecules with TiO_2 surface. This spectral broadening and red shift is attributed to the formation of aggregated dye molecules in the condensed state. Using Indolene class of dye D-205, Horiuchi et al have demonstrated the formation the J-aggregates upon adsorption of this dye on the surface of the mesoporous TiO_2 [31]. On the other hand, SQ-110 shows intense and narrow absorption of light mainly in the far-red wavelength (550-700) nm having λ_{max} at 650 nm with ε of 2.16×10^5 $dm^3mol^{-1}cm^{-1}$, which is about one order of magnitude higher as compared to D-35. At the same time, in solution state, it also shows a vibronic shoulder around 600 nm, which is a typical characteristic of squaraine dyes. This vibronic shoulder is associated with molecular aggregation and get highly pronounced upon the molecular aggregation. Observation of such a higher ε of SQ-110 as compared to D-35 is associated with the high electron density on the cyclobutene ring of the central squaric acid core [32]. Planarity of the molecular framework due to the extended π-conjugation promotes the delocalized intramolecular charge transfer from the HOMO of donor moiety (indole ring) to the LUMO of the acceptor (squaric acid) resulting in to the high ε value [33].

In the solid-state, SQ-110 exhibits small bathochromically shifted λ_{max} at 655 nm along with spectral broadening. Planarity of the dye molecule facilitates the formation of dye aggregates leading to the pronounced enhancement of vibronic shoulder resulting in to clearly visible peak around 610

nm upon adsorption of the dye on TiO_2 [34]. This spectral broadening in solid-state is due to the deprotonation of the acidic anchoring group (–COOH) and its interaction with TiO_2 in the condensed state. Spectral broadening towards lower wavelength region than monomeric absorption peak in solution and enhancement in the intensity of vibronic shoulder has been attributed to the formation of H-aggregates in the squaraine dyes [35, 36]. Therefore, ratio between absorbance of the H-aggregate band (around 610 nm) and the monomer band in solution (650) can be used as indicator of extent of H-aggregation [37]. In his work, Yum et al, clearly demonstrated that extent of H-aggregates of squaraine dye on the mesoporous TiO_2 decreases as function of added fraction of bulky CDCA in dye solution as co-adsorber which prevents the dye aggregation. In the present case, SQ-110 exhibits a dye aggregation of 0.87 upon its adsorption to mesoporous TiO_2 as shown in the Fig. 3, which is a bit lower as compared to the report of 0.95 by Yum et al. This could be attributed to the fact that in their squaraine dye they have used one -methyl and one –octyl group as alkyl substituents while in SQ-110, there are two dimethyl-octyl branched and long alkyl chains hindering the self-aggregation of the dyes. A perusal of the absorption spectra of D-35 and SQ-110 clearly corroborates that they exhibit very good complementary electronic absorption, which becomes more pronounced in the solid-state. This suggests that dye cocktail of these two dyes are expected to provide much-improved light absorption in the entire visible wavelength region as compared to the respective single dyes.

The electronic absorption spectra of dye cocktails of D-35 and SQ-110 in the different molar ratios in ethanol solution as well as on mesoporous TiO_2 film are shown in the Fig. 4. Absorption spectra in the solution exhibit absorption in the 400 nm-500 nm and 550 nm-700 nm associated with the dyes D-35 and SQ-110, respectively. As expected, increase in the ratio of D-35 leads to the corresponding decrease in the light absorption associated with SQ-110 and thus ascertains the need for higher fraction of D-35 in the dye cocktail owing to its lower ε as shown in the Fig. 3. This also suggests for the obvious need of dye cocktails of D-35 and SQ-110 in 4:1 ratio towards the appreciable

wide photon-harvesting window covering the entire visible wavelength region. In the solution-state, absorption spectral feature of dye cocktail is the reflection of presence of both of the dyes and governed quantitatively by their ratio and relative ε values, which can be clearly seen in the Fig. 4. On the other hand, electronic absorption in the solid-state are more realistic representation of the situation occurring in the real DSSC. This is controlled by the nature of dyes, their interaction with the TiO_2 surface and diffusion rate in the mesoporous TiO_2 as reported by our group previously [38, 39]. Especially, it becomes more important in the case of dye cocktails of two or more entirely different dyes and clarifies the actual optimization and selection of optimum ratio of the dyes in the cocktail.

In order to probe differential spectral features and optimization of ratio of individual dyes in the dye cocktail, other parameters like concentration, temperature, thickness of the mesoporous TiO_2 layer and dye adsorption time were fixed to be 0.1 mM, 30^{o}C, 3 μm and 30 min., respectively. Considering the absorbance of dye cocktails at 460 nm and 650 nm corresponding to D-35 and SQ-110, respectively, on the mesoporous TiO_2 (shown by solid lines), we can predict the presence of respective dyes. In this context, solid-state electronic absorption spectra normalized with respect of SQ-110 indicates the relative presence of respective dyes by comparing the relative absorbance at 460 nm and 650 nm associated with the D-35 and SQ-110, respectively taking their respective ε values in to consideration. It can be clearly seen from the Fig. 4 that in spite of the presence of 20 % and 50 % molar fractions of D-35 in the (1:4) and (1:1) cocktail solutions, it is present in the 26 % and 64 %, respectively with respect to SQ-110 on the mesoporous TiO_2. On the other hand, in the dye cocktail ratio (4:1), there is appreciably good light absorption in the 400 nm-550 nm associated with D-35 due it its highly enhanced extent (90 %) on the mesoporous TiO_2. About an order of magnitude lower ε of D-35 compared to that of SQ-110, justifies the utilization of this dye cocktail for facile photon harvesting by both of the dyes in the entire visible wavelength region. It is interesting and worth to mention here that extent of H-aggregation of SQ-110 was estimated to be 0.81, 0.63 and 0.54 for the dye cocktails (1:4), (1:1) and (4:1), respectively, indicating

a dual role of D-35 like co-adsorber and dye de-aggregating agent like CDCA in the dye cocktail utilized for present investigation.

3.2 Energy Band diagram

Sensitizing dyes are undoubtedly one of the most important components of the DSSC and their logical selection in terms of light absorption window and most importantly, energetics should be taken in to consideration for the functioning of the device. LUMO energy level of the dye with respect to the conduction band (CB) of the mesoporous wide band gap semiconductor and its HOMO energy level with respect to the redox electrolyte should be controlled carefully for the facile electron injection and dye regeneration, respectively. LUMO energy level of the dye should be sufficiently above the quasi Fermi level of TiO_2 in order to afford the necessary driving force for electron injection. Pandey et al have recently reported that a minimum energy barrier of 0.16 eV is necessary for the electron injection from the excited dye molecules to the CB of TiO_2 utilizing different squaraine dyes [40]. Energy band diagram for different components of DSSCs such as electrode, sensitizing dyes and electrolyte used for present investigation is shown in the Fig. 5. To construct this, HOMO and LUMO energy levels of sensitizing dye D-35 are taken from the report by Gabrielsson et al [41]. Redox potential of cobalt electrolyte $Co(bpy)^{2+/3+}$ redox couple has been reported to be 0.57 V vs. NHE, which translates in to -5.00 eV with respect to the energy from vacuum level [42]. At the same time, CB of TiO_2 was taken to be -4.00 eV considering the most negative quasi Fermi level corresponding to the flat band potential of TiO_2 (0.7 V vs. SCE) [43].

We can see from the Fig. 5 that LUMO level of squaraine dye SQ-110 is -3.22 eV having a driving force of 0.78 eV while it was even higher at -2.99 eV for D-35 with an energy difference of 1.01 eV from CB of TiO_2. Such a high driving force ensures the facile electron injection from the photoexcited dye to the CB of TiO_2. At the same time, existence of energy cascade between sensitizing dyes and CB of TiO_2 offers an additional pathway of electron injection from the excited state of D-35 to CB of TiO_2

via LUMO of SQ-110 promoting the facile electron injection. On the other hand, there is a good congruency between the HOMO level of the dyes and the redox potential of the cobalt complex electrolyte, which indicates the regeneration of oxidized dyes completing the electron flow cycle during functioning of the DSSC. It can be seen that SQ-110 bears an electron donating methoxy group along with the presence of two long and branched alkyl chains, which leads to upward shift of energy levels of this dye [44]. It is interesting to note that SQ-110 is being regenerated even with a very low driving force of 0.1 eV with the cobalt complex electrolyte used in this work. Dye regeneration is justified by the observation of good photovoltaic performances of DSSCs using this dye alone as well as in the dye cocktails. Figure 6 exhibits the electronic absorption and fluorescence emission spectra of sensitizers in ethanol solution.

3.4 Energy Transfer and Time Resolved Fluorescence Studies

Apart from utilization of dye-cocktails aiming towards panchromatic photon harvesting, approaches like utilization fluorescence resonance energy transfer (FRET) for realization of FRET-enhanced DSSCs has also got momentum in the recent past [45, 46]. FRET has been reported to be a valuable tool to achieve a strong and wide wavelength photon harvesting leading to enhanced Jsc without having detrimental effects on the other key photovoltaic parameters like Voc and fill factor as advocated by Basham et al [47]. Significant overlap of absorption spectrum of one sensitizer (acceptor) with and emission spectrum of another sensitizer (acceptor) is one of the primary requirements of realization of the FRET. Since band gap of D-35 is higher as compared to SQ-110 as evident from the energy band diagram (Fig. 5), their might be a possibility of FRET between these two dyes, which might also be useful for FRET enhanced DSSCs especially fabricated using dye-cocktails in this work. Figure 6 (a) exhibits electronic absorption spectra of D-35 and SQ-110 and fluorescence emission spectrum of D-35 in ethanol solution. It can be seen that D-35 exhibits a broad fluorescence emission from 550 nm-750 nm having emission maximum at 630 nm. At the same time, there is very good overlap between the emission spectrum of D-35 with the absorption spectrum of SQ-110 indicating

the possibility of FRET between these two dyes by energy transfer from the excited state of D-35 to the SQ-110 provided that these dyes should be present in the close vicinity. In order to provide close vicinity between the sensitizers and prevent the complexity due to electron injection, we have used wide band gap ZrO_2. A very large band gap (5.0 eV) of ZrO_2 prevents the electron injection and allows us to probe the time resolved fluorescence decays while keeping the adsorbed dyes in the close proximity [48]. Dyes were adsorbed on the mesoporous ZrO_2 (4 μm) from their respective 0.1 mM ethanolic solutions (D-35and dye cocktails) at room temperature for 1 hour in order to have sufficient dye loading. These dye adsorbed ZrO_2 films were subjected to the time resolved fluorescence investigation. Time resolved fluorescence decay for dye-adsorbed ZrO_2 films is shown in the Fig. 6(b) along with the summarization of the excited-state lifetime and its components obtained after 2^{nd} order fitting of the decay curve in the table 1. A perusal of this figure and table 1 clearly indicates that fluoresecence decay becomes faster after the increase in the mole fraction of SQ-110. Average lifetime was found to be decreased from 1.58 ns for D-35 only to 0.58 ns for dye cocktail having D-35 and SQ-110 in 1:4 ratio. A similar type of observation of FRET in the dye cocktail system of porphyrin and squaraine dyes has also been reported by Patwari et al [49]. This could be explained considering occurrence of FRET between the higher band gap dye D-35 working as donor and relatively narrow band gap dye SQ-110 as acceptor. This lead to possibility of FRET enhanced photon to light conversion the present dye cocktail system. In the case of DSSCs fabricated using the dye cocktail of D-35 and SQ-110, there is dual possibility of electron injection from excited dye molecules to TiO2 and energy transfer from the D-35 to SQ-110.

Table 1. Excited-state lifetime for the D-35(donor) adsorbed on ZrO_2 in the absence and presence the SQ-110 (acceptor) in different ratios.

Dye Cocktail (D-35:SQ-110)	**$<\tau>$ (ns)**	**τ_1 (ns)**	**τ_2 (ns)**
100:0	1.58	0.96	2.46
80:20	1.27	0.67	1.99
50:50	0.77	0.38	1.43
20:80	0.58	0.21	1.03

3.5 Photovoltaic Characterization

It has been reported that utilization of cobalt electrolyte in DSSCs needs careful consideration about photoanode fabrication in terms of use of relatively thin mesoporous TiO_2 layer and surface passivation of both of conducting substrate as well as mesoporous TiO_2 owing to enhanced charge recombination [50]. A compact layer of wide band gap metal oxides retards the charge recombination between the injected electrons of TiO_2 and oxidized dyes as well as electrolytic species. It has been widely accepted and verified by our group that surface treatment on both of the FTO and mesoporous TiO_2 is necessary to get the optimum performance of DSSCs based on single electron transfer outer-sphere cobalt redox electrolytes [51]. In this work, three different most widely used metal oxides such as TiO_2, MgO and Al_2O_3 have been utilized for the surface passivation of mesoporous TiO_2 before dye adsorption by solution based approaches. Mesoporous TiO_2 surface was passivated by single as well as multilayers of compact metal oxides as schematically shown in the Fig. 7 in order to investigate the implication of surface passivation on the final device performance.

3.5.1 Surface passivation of mesoporous TiO_2 using different metal oxides

In order to investigate the implication of surface treatment of mesoporous TiO_2 with different metal oxides, DSSCs were fabricated using photoanode sensitized with a dye-cocktail of D-35 and SQ-110 (8:2) based on superior spectral sensitivity as shown in the Fig. 4. FTO surface treatment to form compact TiO_2 as a charge recombination blocking layer (CRBL) was done using aqueous $TiCl_4$ and kept the same in all of the cases. Photovoltaic characteristics of DSSCs fabricated using photoanodes, where mesoporous TiO_2 was passivated with compact layer of different metal oxides has been shown in the Fig. 8(a) along with photovoltaic parameters summarized in the table 2. Amongst the different metal oxides utilized, surface passivation employing $TiCl_4$ to form compact TiO_2 was par excellent with a power conversion efficiency (PCE) of 4.8 % under simulated solar irradiation.

Table 2. Photovoltaic parameters for the DSSCs utilizing photoanodes fabricated using surface passivation of mesoporous TiO_2 by different type of compact metal oxides. Data shown in the parentheses are average values and standard deviations in the photovoltaic parameters for four independent devices.

Surface treatment	Jsc (mA/cm^2)	Voc (V)	FF	Efficiency (%)
$TiCl_4$	10.36 (10.49 ± 0.35)	0.67 (0.68±0.01)	0.68 (0.65 ± 0.04)	4.78 (4.75 ± 0.23)
MgO	8.90 (8.24 ± 0.70)	0.72 (0.72±0.01)	0.68 (0.63 ± 0.03)	4.45 (3.84 ± 0.55)
Al_2O_3	4.65 (4.61 ± 0.07)	0.66 (0.65 ± 0.01)	0.49 (0.47 ± 0.02)	1.52 (1.42 ± 0.09)

Surface passivation using compact MgO although functions as better CRBL as observed by enhanced open circuit voltage (Voc) but hampered short-circuit current density (Jsc) ultimately results in to decreased overall PCE to 4.4 % as shown in the table 2. Compact Al_2O_3 as CRBL was not found to be good in our case owing to drastically decreased Jsc and no benefit on Voc enhancement. Therefore, as a single compact oxide CRBL, TiO_2 exhibits the optimum performance and this could be associated with the dual role of compact TiO_2. Firstly, there is an enhancement in Jsc, which is attributed to the increased surface area for more dye to be adsorbed and secondly, the ultrathin TiO_2 layer functions as a CRBL towards back electron transfer [29]. Photocurrent action spectra also known as variation of incident photon to current conversion efficiency (IPCE) as a function of wavelength was also measured and shown in the Fig. 8(b). Spectral response clearly reveals the enhanced photosensitization by both of the dyes for the photoanodes passivated with compact TiO_2 and is in accordance with the results of improved Jsc shown in the Fig. 8(a). In order to further confirm the differential surface passivation by different metal oxide layers, EIS was performed by applying a forward bias voltage near to open-circuit voltage in each case as shown in Fig. 8 (c). The EIS pattern can be broadly divided into three regions, R1- resistance due to FTO/TiO_2 interface, R2- resistance associated with the charge transfer at the counter electrode and R3- resistance to recombination at the TiO_2/dye/electrolyte interface [52, 53]. According to the result obtained, there was almost no difference in the value of R1 for each device, which is obvious because of the same photoanode in all the cases. Similarly, no significant difference was seen for R2, therefore, the major role

was due to R3, which can be clearly answered by the difference in passivation by metal oxide layers. Therefore, TiO_2 and MgO clearly exhibits better passivation then Al_2O_3, which was reflected in I-V characteristics as well.

Considering the pros and cons of compact single layer surface passivation by TiO_2 and MgO, it raised the curiosity to probe the influence of multiple layer of compact oxide surface passivation on the photovoltaic performance of DSSCs thus fabricated. To accomplish this, first $TiCl_4$ surface treatment was conducted on both of the FTO and mesoporous TiO_2 followed by 2nd surface passivation of the mesoporous TiO_2 by MgO and Al_2O_3 to make bilayer surface treated electrode using magnesium ethoxide and Aluminum isopropoxide, respectively. One more set of photoanodes were also fabricated using tri-layer surface passivation of the mesoporous TiO_2 where, TiO_2/MgO treated substrate was once more subjected to Al_2O_3 surface treatment, which has been schematically shown in the Fig. 7. These multilayer surface treated electrodes were finally sensitized with the dye cocktail of D-35 and SQ-110 in (4:1) molar ratio for the preparation of respective photoanodes and DSSCs. Photovoltaic characteristics and photocurrent action spectra of these DSSCs were recorded after simulated solar irradiation and has been shown in the Fig. 9. At the same time, photovoltaic parameters deduced from the photovoltaic measurement are summarized in the table 3.

Table 3. Photovoltaic parameters for the DSSCs utilizing photoanodes fabricated by surface passivation of mesoporous TiO_2 using multiple layer of different type of compact metal oxides. Data shown in the parentheses are average values and standard deviations in the photovoltaic parameters for four independent devices.

Surface treatments	Jsc (mA/cm^2)	Voc (V)	FF	Efficiency (%)
TiO_2/MgO	12.50 (11.21 ± 0.34)	0.68 (0.72 ± 0.01)	0.63 (0.68 ± 0.02)	5.40 (5.6 ± 0.26)
TiO_2/Al_2O_3	11.06 (9.13 ± 1.84)	0.65 (0.64 ± 0.01)	0.61 (0.53 ± 0.07)	4.48 (3.28 ± 1.26)
TiO_2/MgO/Al_2O_3	11.01 (8.97 ± 2.04)	0.66 (0.64 ± 0.02)	0.47 (0.49 ± 0.04)	3.43 (2.85 ± 0.64)

Figure 9(a) and table 3 clearly depicts that a bilayer surface treatment consisting of TiO_2/MgO on mesoporous TiO_2 outperforms as compared to both of the TiO_2/Al_2O_3 bilayer and TiO_2/MgO/Al_2O_3 tri-layer surface treatments. A pronounced enhancement in Jsc up to 12.50 mA/cm^2 in TiO_2/MgO treated photoanodes was observed from 10.36 mA/cm2 and 8.90 mA/cm^2 for TiO_2 and MgO single surface treatments, respectively (Fig. 8, table 2). This increased Jsc for the TiO_2/MgO bilayer surface devices was compared to other surface treatments was further supported by photocurrent action spectra shown in the Fig. 9(b), where photon-harvesting corresponding to both of the sensitizer were increased. This demonstrates the superiority of these TiO_2/MgO bilayer surface treatments, which could be attributed to the facile charge injection due to electron tunneling rather than recombination [54]. On the contrary, Aluminum isopropoxide treatment to form compact Al_2O_3 on the mesoporous TiO_2 photoanode based DSSCs did not perform well either for bilayer or tri-layer surface treatments. Poor performance of the TiO_2/MgO/Al_2O_3 tri-layer surface passivation might be associated with the excessive thicketing of the compact layer on the mesoporous TiO_2 as indicated by highly suppressed fill factor (FF) of 0.47 as shown in the table 3. Herein also, to further support the role of passivation and its implication on the observed photovoltaic performances of the fabricated solar cells, EIS measurement was also conducted and results are shown in Fig. 9(c). A bilayer combination of surface treatment using TiO_2/MgO was passivating more effectively than bilayer of TiO_2/Al_2O_3. Furthermore, it was noticed that when a third layer of Al_2O_3 was deposited on top of TiO_2/MgO, there was drastic reduction in value of R3. This indicates alumina layer is not effective for surface passivation, rather works like an insulator opposing the forward injection process leading to poorest solar cell performance as clearly being reflected in the I-V characteristics.

3.5.2 Effect of FTO surface passivation

In the previous section, surface passivation of mesoporous TiO_2 layer by various metal oxides was conducted keeping most widely utilized $TiCl_4$ treated FTO as conducting substrate. Encouraged by optimized surface passivation of mesoporous TiO_2 using compact TiO_2/MgO bilayers, surface passivation

of conducting FTO substrate by single and bilayer consisted of compact TiO_2 and Nb_2O_5 was also attempted. To accomplish this, four variations consisted of single layer as well as bilayer surface treatment of FTO such as TiO_2, Nb_2O_5, TiO_2/Nb_2O_5 and Nb_2O_5/TiO_2 were conducted using aqueous $TiCl_4$, and Niobium butoxide in isopropanol. It has been reported that Nb_2O_5 forms an insulating barrier owing to its very large band gap and functions as not only CRBL but also plays a significant role in the upward shift of TiO_2 conduction band edge [55]. These surface treated FTO substrates were utilized for the photoanode fabrication by optimized TiO_2/MgO bilayer surface treatment of mesoporous TiO_2 followed by dye adsorption using a dye cocktail of D-35 and SQ-110 in 4:1 ratio. The photovoltaic characteristics of DSSCs thus fabricated are shown in Fig. 10 along with summarized photovoltaic parameters in table 4.

Table 4. Photovoltaic parameters for the DSSCs utilizing photoanodes fabricated by surface passivation by surface passivation of FTO using single and bilayers of compact metal oxides. Data shown in the parentheses are average values and standard deviations in the photovoltaic parameters for four independent devices.

Surface treatments	Jsc(mA/cm^2)	Voc (V)	FF	Efficiency (%)
Nb_2O_5 only	6.38 (6.38±1.27)	0.33 (0.35±0.05)	0.38 (0.41±0.05)	0.81 (0.92±0.37)
Nb_2O_5/TiO_2	6.90 (6.24±0.61)	0.41 (0.41±0.02)	0.47 (0.48±0.02)	1.35 (1.26±0.09)
TiO_2 only	12.50 (11.28±1.27)	0.68 (0.63±0.05)	0.63 (0.58±0.05)	5.40 (5.15±0.35)
TiO_2/Nb_2O_5	10.44 ((9.8±0.56))	0.68 (0.64±0.05)	0.60 (0.52±0.06)	4.29 (3.57±0.79)

A perusal of this figure and table clearly corroborates that single layer of compact TiO_2 on FTO provided best photovoltaic performance with a Jsc of 12.50 mA/cm^2, Voc of 0.68 V, FF of 0.63 leading to PCE of 5.40 %. On the other hand, direct surface treatment of FTO forming Nb_2O_5 performs very poor, where all of the device parameters decreased drastically. Such a poor performance of DSSCs by Nb_2O_5 surface treatment of FTO indicates a very strong interaction of Niobium butoxide with FTO. This strong interaction between FTO and Nb_2O_5, probably leads to the formation of very thick insulating barrier. This was further verified by the recovery of device performance when Nb_2O_5 layer was coated on to compact

TiO_2 layer on FTO in the bilayer device. It seems that we had probably taken too high concentration of niobium butoxide solution (20 mM) based on protocol of MgO and Al_2O_3, which may not be similarly applicable for FTO surface treatments.

3.3.3 Influence of dye cocktail ratio and top scattering layer

Results on optimization of surface passivation on FTO as well mesoporous TiO_2 have indicated that single layer of compact TiO_2 and a bilayer of TiO_2/MgO surface treatments are optimum for the surface passivation of FTO and mesoporous TiO_2, respectively. As a final optimization, 3 μm scattering layer using large particle size (400 nm) TiO_2 (PST-400) was further applied on TiO_2/MgO surface passivated mesoporous TiO_2 for the photoanode fabrication. DSSCs were then fabricated by sensitizing the mesoporous TiO_2 with dyes D-35, SQ-110 and their dye cocktails in different molar ratios such as (1:4), (1:1) and (4:1) along with $Co(bpy)^{2+/3+}$ redox electrolyte. Photovoltaic characteristics DSSCs thus prepared after simulated solar irradiation are shown in the Fig. 11 along with the photovoltaic parameters summarized in the table 5.

Table 5. Photovoltaic parameters for the for the DSSCs fabricated utilizing optimized surface passivated photoanodes sensitized with D-35, SQ-110 and their dye cocktails in different molar ratios. Data shown in the parentheses are average values and standard deviations in the photovoltaic parameters for four independent devices.

Sensitizing Dyes	Jsc (mA/cm^2)	Voc (V)	FF	Efficiency (%)
SQ-110	7.13 (6.68 ± 0.47)	0.50 (0.51 ± 0.03)	0.54 (0.51 ± 0.03)	1.92 (1.88 ± 0.08)
D-35	7.39 (7.14 ± 0.22)	0.84 (0.86 ± 0.01)	0.58 (0.57 ± 0.01)	3.63 3.50 ± 0.10
D-35:SQ-110 (1:4)	7.63 (6.85 ± 0.73)	0.65 (0.63 ± 0.01)	0.51 (0.47 ± 0.04)	2.53 2.09 ± 0.37
D-35:SQ-110 (1:1)	12.07 (11.66 ± 0.41)	0.68 (0.66 ± 0.02)	0.68 (0.63 ± 0.05)	5.70 4.94 ± 0.52
D-35:SQ-110 (4:1)	14.61 (13.77 ± 0.72)	0.72 (0.73 ± 0.01)	0.68 (0.65 ± 0.03)	7.23 6.69 ± 0.46

A perusal of photon harvesting by individual dyes D-35 and SQ-110 as shown in the Fig. 11(b) clearly corroborates that they complement each other and their dye cocktail leads to wide wavelength photon harvesting in the entire visible wavelength region, which is in agreement with solid-state electronic absorption spectra shown in the Fig. 4. D-35 has been widely reported as well as observed in this present work that it is a good sensitizer working very well with cobalt complex electrolytes (Fig. 11b, table 5) but its narrow photon harvesting window needs its association with another far-red to NIR photon harvesting dye in order to have photon harvesting in the wide wavelength region. In spite of a good deal of research works on visible light harvesting dyes in combination with cobalt redox shuttle as electrolyte, there are very few reports on DSSCs based on NIR dyes in combination with cobalt complex electrolyte [56]. In fact, previously, we have also challenged this issue using model squaraine dyes in combination with cobalt electrolyte but very poor efficiency (<0.2 %) indicated the need for strict surface passivation along with suitable molecular design of the sensitizers [57]. It can be seen from the Fig. 11(a) and table 5 that our newly designed SQ-110 functions well with cobalt electrolyte having PCE of 1.92 % along with photon harvesting mainly in the far-red region. This could be credited to the effective surface passivation of both of the FTO and TiO_2 along with the introduction of two branched long alkyl chain to assist the additional TiO_2 surface passivation thus prohibiting the charge recombination between electrons injected in TiO_2 and oxidized electrolyte [58].

It is interesting to see from Fig. 11(a, b) and table 5 that in the dye cocktail sensitized photoanodes, individual dyes complement each other where, lower Voc of SQ-110 is enhanced in the presence of D-35. At the same time, photon harvesting in the far-red region which was absent in D-35 is remarkably improved due to presence of SQ-110. Huge differences in the molar extinction co-efficient of constituent dyes D-35 and SQ-110 as shown in the figures (3, 4) clearly indicates the need for their optimum ratio in the dye cocktail in order to harness their utmost benefits. A dye cocktail solution of D-35 and SQ-110 in (1:4) molar ratio although exhibit photon harvesting in both of the visible (due to D-35) and far-red (due to SQ-110) wavelength region but overall PCE was only 2.53 %, which is although

higher than SQ-110 (1.92 %) but lower than D-35 (3.63 %). This could be attributed to the presence relatively smaller extent (26 %) of D-35 molecules hampering the photon harvesting in lower wavelength region, which is clear from the solid-state electronic absorption spectra shown in the Fig. 4 also. In the section 3.1 it has been discussed that increasing the mole fraction of D-35 in the dye cocktails in the ratio (1:1) and (4:1) led to an appreciable enhancement in its fraction up to 64 % and 90 % on the mesoporous TiO_2, respectively. At the same time, increasing the extent of D-35 not only leads to facile photon harvesting in the 300 nm – 550 nm by D-35 but also leading to pronounced suppression of H-aggregation of SQ-110 from 0.81 for the dye cocktail (4:1) to 0.54 for the dye cocktail (1:4). This pronounced suppression of dye aggregation of SQ-110 by D-35 along with its presence in higher extent (90 %) in the dye cocktail led to the best photovoltaic performance of 7.23 % under simulated solar irradiation. This enhanced performance of DSSC using the (4:1) dye cocktail of D-35 and SQ-110 is associated with both of the improved Jsc as well as Voc (table 5) and photon harvesting in entire visible wavelength region associated with both of the respective dyes (Fig. 11b).

One can argue here that why in the dye cocktails especially with the ratio (1:1) and (4:1) photon harvesting is higher than respective individual dyes D-35 and SQ-110 as depicted by photocurrent action spectra shown in the Fig. 11(b). This could be attributed to suppression of dye aggregation of SQ-110 by D-35 and promotion of J-aggregation in D-35 by SQ-110 on the mesoporous TiO_2. Although there is still debate about the aggregation behavior of D-35 on the TiO_2 surface but based on experimental as well as theoretical quantum chemical calculations, it has been demonstrated that there is J-aggregate formation by D-35 and small butoxy substituent is not enough to prevent the dye aggregation even using D-35 and CDCA in 1:50 ratio [59, 60]. Formation of J-aggregates are expected to broaden the spectral response and could be responsible for the enhanced Jsc. In the present case dye cocktails, SQ-110 seems to functions as J-aggregate promoter like CDCA resulting in to enhanced photon harvesting associated with D-35. On the other hand, D-35 has a dual role of complementary

light harvesting co-sensitizer as well as dye H-aggregate preventer of SQ-110 leading to enhanced photon harvesting in the far-red region as compared to the single dye. Another reason could be associated with the fluorescence enhanced energy transfer from D-35 to SQ-110 as discussed in the section 3.4 previously. Apart from increase in the light harvesting window, presence of both of dyes favours the occurrence of FRET from D-35 to SQ-110 leading significant increase in photocurrent. In fact, Patwari et al has also reported enhancement mainly in Jsc for the DSSCs fabricated using dye cocktails of porphyrin and squaraine dyes without affecting the Voc and explained taking FRET promoted enhanced photon harvesting in to consideration [49]. Pronounced photon harvesting by dye cocktails as compared to their respective individual dye counterparts have been reported by Ogura et al and Lin et al [61, 62] also.

4. Conclusion

A novel far-red sensitive unsymmetrical squaraine dye (SQ-110) bearing direct-carboxy functionalized indole ring and branched long alkyl substituent has been successfully, synthesized, characterized and used as sensitizer towards application in the DSSC using cobalt complex redox electrolyte. A commercial dye D-35 having complementary light absorption with SQ-110 has been utilized to sensitize the mesoporous TiO_2 with the dye-cocktails in different molar ratios leading to not only improved photon harvesting as compared to individual constituent dyes but also improved wide-wavelength photon harvesting from visible to far-red region of the spectrum. Considering the importance of surface passivation towards suppression of charge recombination especially in the DSSCs based on cobalt electrolytes, surface passivation of both of the FTO as well as mesoporous TiO_2 has been systematically conducted and their implication on the photovoltaic performance was investigated in detail. It has been demonstrated that a compact TiO_2 on FTO and a bilayer TiO_2/MgO surface passivation was necessary for getting the optimum DSSC performance. A DSSC fabricated with dye cocktail of D-35 and SQ-110 in (4:1) ratio as sensitizer in combination $Co(bpy)^{2+/3+}$ redox electrolyte exhibited a Jsc of 14.61 mA/cm^2, Voc of 0.72 V and FF of 0.68 leading to PCE of 7.23 %,

which is much higher than the individual constituent dyes. In the present dye-cocktail DSSCs, mutual control of dye aggregation, complementary photon harvesting and FRET between two dyes are found to be responsible synergistically enhanced photon harvesting in the wide wavelength region. Interestingly, successful dye regeneration of SQ-110 even with a very small driving force of 0.10 eV indicates the possibility of further molecular design of novel sensitizers having the capability of photon harvesting in the NIR wavelength region.

References

[1] A. Demirbas, Potential applications of renewable energy sources, biomass combustion problems in boiler power systems and combustion related environmental issues, Progress in energy and combustion science, 31 (2005) 171-192.

[2] C. Strümpel, M. McCann, G. Beaucarne, V. Arkhipov, A. Slaoui, V. Švrček, C. Del Cañizo, I. Tobias, Modifying the solar spectrum to enhance silicon solar cell efficiency—An overview of available materials, Solar energy materials and solar cells, 91 (2007) 238-249.

[3] R.W. Miles, G. Zoppi, I. Forbes, Inorganic photovoltaic cells, Materials today, 10 (2007) 20-27.

[4] J. Britt, C. Ferekides, Thin-film CdS/CdTe solar cell with 15.8% efficiency, Applied Physics Letters, 62 (1993) 2851-2852.

[5] S.H. Park, A. Roy, S. Beaupré, S. Cho, N. Coates, J.S. Moon, D. Moses, M. Leclerc, K. Lee, A.J. Heeger, Bulk heterojunction solar cells with internal quantum efficiency approaching 100%, Nature photonics, 3 (2009) 297-302.

[6] I. McConnell, G. Li, G.W. Brudvig, Energy conversion in natural and artificial photosynthesis, Chemistry & biology, 17 (2010) 434-447.

[7] B. O'regan, M. Grätzel, A low-cost, high-efficiency solar cell based on dye-sensitized colloidal TiO_2 films, nature, 353 (1991) 737-740.

[8] B. Zhang, H. Yuan, X. Zhang, D. Huang, S. Li, M. Wang, Y. Shen, Investigation of regeneration kinetics in quantum-dots-sensitized solar cells with scanning electrochemical microscopy, ACS applied materials & interfaces, 6 (2014) 20913-20918.

[9] Y. Wang, E.L. Runnerstrom, D.J. Milliron, Switchable materials for smart windows, Annual review of chemical and biomolecular engineering, 7 (2016) 283-304.

[10] M. Pastore, F. De Angelis, Intermolecular interactions in dye-sensitized solar cells: a computational modeling perspective, The journal of physical chemistry letters, 4 (2013) 956-974.

[11] Y. Cui, Y. Wu, X. Lu, X. Zhang, G. Zhou, F.B. Miapeh, W. Zhu, Z.-S. Wang, Incorporating benzotriazole moiety to construct D–A− π–A organic sensitizers for solar cells: significant enhancement of open-circuit photovoltage with long alkyl group, Chemistry of Materials, 23 (2011) 4394-4401.

[12] Y. Wu, W. Zhu, Organic sensitizers from D–π–A to D–A–π–A: effect of the internal electron-withdrawing units on molecular absorption, energy levels and photovoltaic performances, Chemical Society Reviews, 42 (2013) 2039-2058.

[13] D.W. Chang, H.J. Lee, J.H. Kim, S.Y. Park, S.-M. Park, L. Dai, J.-B. Baek, Novel quinoxaline-based organic sensitizers for dye-sensitized solar cells, Organic letters, 13 (2011) 3880-3883.

[14] M. Jørgensen, K. Norrman, S.A. Gevorgyan, T. Tromholt, B. Andreasen, F.C. Krebs, Stability of polymer solar cells, Advanced materials, 24 (2012) 580-612.

[15] M. Kimura, H. Nomoto, N. Masaki, S. Mori, Dye Molecules for Simple Co-Sensitization Process: Fabrication of Mixed-Dye-Sensitized Solar Cells, Angewandte Chemie International Edition, 51 (2012) 4371-4374.

[16] J.J. Cid, J.H. Yum, S.R. Jang, M.K. Nazeeruddin, E. Martínez-Ferrero, E. Palomares, J. Ko, M. Grätzel, T. Torres, Molecular Cosensitization for Efficient Panchromatic Dye-Sensitized Solar Cells, Angewandte Chemie, 119 (2007) 8510-8514.

[17] D. Zhou, Q. Yu, N. Cai, Y. Bai, Y. Wang, P. Wang, Efficient organic dye-sensitized thin-film solar cells based on the tris (1, 10-phenanthroline) cobalt (II/III) redox shuttle, Energy & Environmental Science, 4 (2011) 2030-2034.

[18] J.J. Nelson, T.J. Amick, C.M. Elliott, Mass transport of polypyridyl cobalt complexes in dye-sensitized solar cells with mesoporous TiO2 photoanodes, The Journal of Physical Chemistry C, 112 (2008) 18255-18263.

[19] S. Carli, L. Casarin, S. Caramori, R. Boaretto, E. Busatto, R. Argazzi, C.A. Bignozzi, A viable surface passivation approach to improve efficiency in cobalt based dye sensitized solar cells, Polyhedron, 82 (2014) 173-180.

[20] E. Palomares, J.N. Clifford, S.A. Haque, T. Lutz, J.R. Durrant, Control of charge recombination dynamics in dye sensitized solar cells by the use of conformally deposited metal oxide blocking layers, Journal of the American Chemical Society, 125 (2003) 475-482.

[21] A. Merazga, F. Al-Subai, A.M. Albaradi, A. Badawi, A.Y. Jaber, A.A.B. Alghamdi, Effect of sol–gel MgO spin-coating on the performance of TiO 2-based dye-sensitized solar cells, Materials Science in Semiconductor Processing, 41 (2016) 114-120.

[22] G. de Miguel, M. Ziółek, M. Zitnan, J. Organero, S. Pandey, S. Hayase, A. Douhal, Photophysics of H-and J-aggregates of indole-based squaraines in solid state, The Journal of Physical Chemistry C, 116 (2012) 9379-9389.

[23] K.-L. Wu, A.J. Huckaba, J.N. Clifford, Y.-W. Yang, A. Yella, E. Palomares, M. Grätzel, Y. Chi, M.K. Nazeeruddin, Molecularly engineered Ru (II) sensitizers compatible with cobalt (II/III) redox mediators for dye-sensitized solar cells, Inorganic chemistry, 55 (2016) 7388-7395.

[24] S.M. Feldt, E.A. Gibson, E. Gabrielsson, L. Sun, G. Boschloo, A. Hagfeldt, Design of organic dyes and cobalt polypyridine redox mediators for high-efficiency dye-sensitized solar cells, Journal of the American Chemical Society, 132 (2010) 16714-16724.

[25] Y. Hao, Y. Saygili, J. Cong, A. Eriksson, W. Yang, J. Zhang, E. Polanski, K. Nonomura, S.M. Zakeeruddin, M. Gratzel, Novel blue organic dye for dye-sensitized solar cells achieving high efficiency in cobalt-based electrolytes and by co-sensitization, ACS applied materials & interfaces, 8 (2016) 32797-32804.

[26] H. Li, M. Pang, B. Wu, J. Meng, Synthesis, crystal structure and photochromism of a novel spiro [indoline–naphthaline] oxazine derivative, Journal of Molecular Structure, 1087 (2015) 73-79.

[27] T. Inoue, S.S. Pandey, N. Fujikawa, Y. Yamaguchi, S. Hayase, Synthesis and characterization of squaric acid based NIR dyes for their application towards dye-sensitized solar cells, Journal of Photochemistry and Photobiology A: Chemistry, 213 (2010) 23-29.

[28] M.J. Marchena, G. de Miguel, B. Cohen, J.A. Organero, S. Pandey, S. Hayase, A. Douhal, Real-time photodynamics of squaraine-based dye-sensitized solar cells with iodide and cobalt electrolytes, The Journal of Physical Chemistry C, 117 (2013) 11906-11919.

[29] P. Sommeling, B. O'regan, R. Haswell, H. Smit, N. Bakker, J. Smits, J. Kroon, J. Van Roosmalen, Influence of a $TiCl_4$ post-treatment on nanocrystalline TiO2 films in dye-sensitized solar cells, The Journal of Physical Chemistry B, 110 (2006) 19191-19197.

[30] K. Kakiage, H. Osada, Y. Aoyama, T. Yano, K. Oya, S. Iwamoto, J.-i. Fujisawa, M. Hanaya, Achievement of over 1.4 V photovoltage in a dye-sensitized solar cell by the application of a silyl-anchor coumarin dye, Scientific reports, 6 (2016) 35888.

[31] T. Horiuchi, H. Miura, K. Sumioka, S. Uchida, High efficiency of dye-sensitized solar cells based on metal-free indoline dyes, Journal of the American Chemical Society, 126 (2004) 12218-12219.

[32] G. Chen, H. Sasabe, T. Igarashi, Z. Hong, J. Kido, Squaraine dyes for organic photovoltaic cells, Journal of Materials Chemistry A, 3 (2015) 14517-14534.

[33] A. Ajayaghosh, Chemistry of squaraine-derived materials: near-IR dyes, low band gap systems, and cation sensors, Accounts of Chemical Research, 38 (2005) 449-459.

[34] A. Eisfeld, J. Briggs, The J-and H-bands of organic dye aggregates, Chemical Physics, 324 (2006) 376-384.

[35] J.-H. Yum, P. Walter, S. Huber, D. Rentsch, T. Geiger, F. Nüesch, F. De Angelis, M. Grätzel, M.K. Nazeeruddin, Efficient far red sensitization of nanocrystalline TiO2 films by an unsymmetrical squaraine dye, Journal of the American Chemical Society, 129 (2007) 10320-10321.

[36] E.L. Unger, A. Morandeira, M. Persson, B. Zietz, E. Ripaud, P. Leriche, J. Roncali, A. Hagfeldt, G. Boschloo, Contribution from a hole-conducting dye to the photocurrent in solid-state dye-sensitized solar cells, Physical Chemistry Chemical Physics, 13 (2011) 20172-20177.

[37] J. Yum, S. Moon, R. Humphry-Baker, P. Walter, T. Geiger, F. Nüesch, M. Grätzel, M. d K Nazeeruddin, Effect of coadsorbent on the photovoltaic performance of squaraine sensitized nanocrystalline solar cells, Nanotechnology, 19 (2008) 424005.

[38] M. Kawano, T. Nishiyama, Y. Ogomi, S.S. Pandey, T. Ma, S. Hayase, Relationship between diffusion of Co 3+/Co 2+ redox species in nanopores of porous titania stained with dye molecules, dye molecular structures, and photovoltaic performances, RSC Advances, 5 (2015) 83725-83731.

[39] Y. Ogomi, S.S. Pandey, S. Kimura, S. Hayase, Probing mechanism of dye double layer formation from dye-cocktail solution for dye-sensitized solar cells, Thin Solid Films, 519 (2010) 1087-1092.

[40] S.S. Pandey, T. Morimoto, N. Fujikawa, S. Hayase, Combined theoretical and experimental approaches for development of squaraine dyes with small energy barrier for electron injection, Solar Energy Materials and Solar Cells, 159 (2017) 625-632.

[41] E. Gabrielsson, H. Ellis, S. Feldt, H. Tian, G. Boschloo, A. Hagfeldt, L. Sun, Convergent/Divergent Synthesis of a Linker-Varied Series of Dyes for Dye-Sensitized Solar Cells Based on the D35 Donor, Advanced Energy Materials, 3 (2013) 1647-1656.

[42] M. Wang, C. Grätzel, S.M. Zakeeruddin, M. Grätzel, Recent developments in redox electrolytes for dye-sensitized solar cells, Energy & Environmental Science, 5 (2012) 9394-9405.

[43] Y. Ogomi, T. Kato, S. Hayase, Dye sensitized solar cells consisting of ionic liquid and solidification, Journal of Photopolymer Science and Technology, 19 (2006) 403-408.

[44] S.S. Pandey, T. Inoue, N. Fujikawa, Y. Yamaguchi, S. Hayase, Substituent effect in direct ring functionalized squaraine dyes on near infra-red sensitization of nanocrystalline TiO2 for molecular photovoltaics, Journal of Photochemistry and Photobiology A: Chemistry, 214 (2010) 269-275.

[45] L. Han, A. Islam, H Chen, C. Malapaka, B. Chiranjeevi, S. Zhang, X. Yang, M. Yanagida, High-efficiency dye-sensitized solar cell with a novel co-adsorbent, Energy and Environmental Science, 5 (2012) 6057–6060**.**

[46] J.W Shiu, Y.C Chang, C.Y. Chan, H.P .Wu, H.Y Hsu, C.L. Wang, C.Y Lin, E.W.G Diau, Panchromatic co-sensitization of porphyrin-sensitized solar cells to harvest near-infrared light beyond 900 nm, Journal of Material Chemistry A, 3 (2015) 1417–1420.

[47] J. Basham, I. G. K. Mor, C. A. Grimes, Förster Resonance Energy Transfer in Dye-Sensitized Solar Cells, American Chemical Society 4 (2010), 1253–1258.

[48] A.V. Emeline, G.N Kuzmin, D. Purevdorj, V.K Ryabchuk, N. Serpone, Spectral dependencies of the quantum yield of photochemical processes on the surface of wide band gap solids. 3. Gas/solid systems, Journal of Physical Chemistry B, 14 (2000) 2989–99.

[49] J. Patwari, S. Sardar1, B. Liu, P. Lemmens, and S. K Pal, Three-in-one approach towards efficient organic dye-sensitized solar cells: aggregation suppression, panchromatic absorption and resonance energy transfer, Beilstein Journal of Nanotechnology, 8 (2017) 1705–1713.

[50] M. Wang, C. Grätzel, S.M. Zakeeruddin, M. Grätzel, Recent developments in redox electrolytes for dye-sensitized solar cells, Energy & Environmental Science, 5 (2012) 9394-9405.

[51] A. Pradhan, M. Saikiran, G. Kapil, S. S. Pandey, S. Hayase, Dye-Sensitized Solar Cells utilizing Far-red Sensitive Dyes in Combination with Cobalt Complex based Redox Electrolyte, J. Phys. Conf. Ser., 2017 (In Press).

[52] T. Hoshikawa, M. Yamada, R. Kikuchi, K. Eguchi, Impedance analysis of internal resistance affecting the photoelectrochemical performance of dye-sensitized solar cells. Journal of Electrochemical Society, 152 (2005) E68-E73.

[53] G. Kapil, J. Ohara, Y. Ogomi, S.S. Pandey, T. Ma, S. Hayase, Fabrication and characterization of transparent conducting oxide-less cylindrical dye-sensitized solar cells. Royal Society of Chemistry: Advances, 4 (2014) 22959-22963.

[54] S.E. Koops, B.C. O'Regan, P.R. Barnes, J.R. Durrant, Parameters influencing the efficiency of electron injection in dye-sensitized solar cells, Journal of the American Chemical Society, 131 (2009) 4808-4818.

[55] E.M. Barea Berzosa, X. Xu, V. González Pedro, T. Ripollés Sanchis, F. Fabregat Santiago, J. Bisquert, Origin of efficiency enhancement in Nb2O5 coated titanium dioxide nanorod based dye sensitized solar cells, (2011).

[56] J.-H. Yum, T.W. Holcombe, Y. Kim, K. Rakstys, T. Moehl, J. Teuscher, J.H. Delcamp, M.K. Nazeeruddin, M. Grätzel, Blue-coloured highly efficient dye-sensitized solar cells by implementing the diketopyrrolopyrrole chromophore, Scientific reports, 3 (2013).

[57] M.J. Marchena, G. de Miguel, B. Cohen, J.A. Organero, S. Pandey, S. Hayase, A. Douhal, Real-time photodynamics of squaraine-based dye-sensitized solar cells with iodide and cobalt electrolytes, The Journal of Physical Chemistry C, 117 (2013) 11906-11919.

[58] J.E. Kroeze, N. Hirata, S. Koops, M.K. Nazeeruddin, L. Schmidt-Mende, M. Grätzel, J.R. Durrant, Alkyl chain barriers for kinetic optimization in dye-sensitized solar cells, Journal of the American Chemical Society, 128 (2006) 16376-16383.

[59] V. Dryza, E.J. Bieske, Does the triphenylamine-based D35 dye sensitizer form aggregates on metal-oxide surfaces?, Journal of Photochemistry and Photobiology A: Chemistry, 302 (2015) 35-41.

[60] V. Dryza, E.J. Bieske, Suppressing Förster Resonance Energy Transfer between Organic Dyes on a co-sensitized Metal Oxide Surface, The Journal of Physical Chemistry C, 118 (2014) 19646-19654.

[61] R.Y. Ogura, S. Nakane, M. Morooka, M. Orihashi, Y. Suzuki, K. Noda, High-performance dye-sensitized solar cell with a multiple dye system, Applied Physics Letters, 94 (2009) 54.

[62] R.Y.-Y. Lin, Y.-S. Yen, Y.-T. Cheng, C.-P. Lee, Y.-C. Hsu, H.-H. Chou, C.-Y. Hsu, Y.-C. Chen, J.T. Lin, K.-C. Ho, Dihydrophenanthrene-based metal-free dyes for highly efficient cosensitized solar cells, Organic letters, 14 (2012) 3612-3615.

Figure Captions

Figure 1. Chemical structures of newly synthesized far-red sensitizing unsymmetrical squaraine dye (SQ-110) (a) and commercial dye D-35 (b).

Figure 2. Synthesis scheme for the synthesis of SQ-110 and intermediates

Figure 3. Electronic absorption of sensitizing dyes D-35 and SQ-110 in ethanol solution and mesoporous TiO_2. Dotted lines represent absorption spectra in the solution while solid lines are respective spectra in solid-state for dyes adsorbed in thin mesoporous TiO_2. Absorption spectra on TiO_2 are normalized with respect to absorption maximum of the respective dyes in solution.

Figure 4. Electronic absorption of dye cocktails of D-35 and SQ-110 in different molar ratios. Dotted lines represent corresponding absorption spectra in the solution while solid lines are respective spectra for the dyes adsorbed on thin film of mesoporous TiO_2. Absorption spectra on TiO_2 are normalized with respect to λ_{max} of the respective dyes in solution.

Figure 5. Energy band diagram for sensitizing dyes SQ-110 and D-35 along with TiO_2 and cobalt complex redox electrolyte.

Figure 6. Electronic absorption and fluorescence emission spectra of sensitizers in ethanol solution exhibiting spectral overlap (a) and time-resolved fluorescence decay for dyes adsorbed on mesoporous ZrO_2 (b).

Figure 7. Schematic representation of surface passivation of mesoporous TiO_2 using compact layer of different metal oxides.

Figure 8. Photovoltaic characteristics (a), photocurrent action spectra (b) and EIS Nyquist plot (c) for the DSSCs utilizing photoanodes fabricated using surface passivation of mesoporous TiO_2 by different type of compact metal oxides.

Figure 9. Photovoltaic characteristics (a), photocurrent action spectra (b) and EIS Nyquist plot (c) for the DSSCs utilizing photoanodes fabricated by surface passivation of mesoporous TiO_2 using multiple layer of different type of compact metal oxides.

Figure 10. Photovoltaic characteristics (a) and photocurrent action spectra (b) for the DSSCs utilizing photoanodes fabricated by surface passivation of FTO using single and bilayers of compact metal oxides.

Figure 11. Photovoltaic characteristics (a) and photocurrent action spectra (b) for the DSSCs fabricated utilizing optimized surface passivated photoanodes sensitized with D-35, SQ-110 and their dye cocktails in different molar ratios.

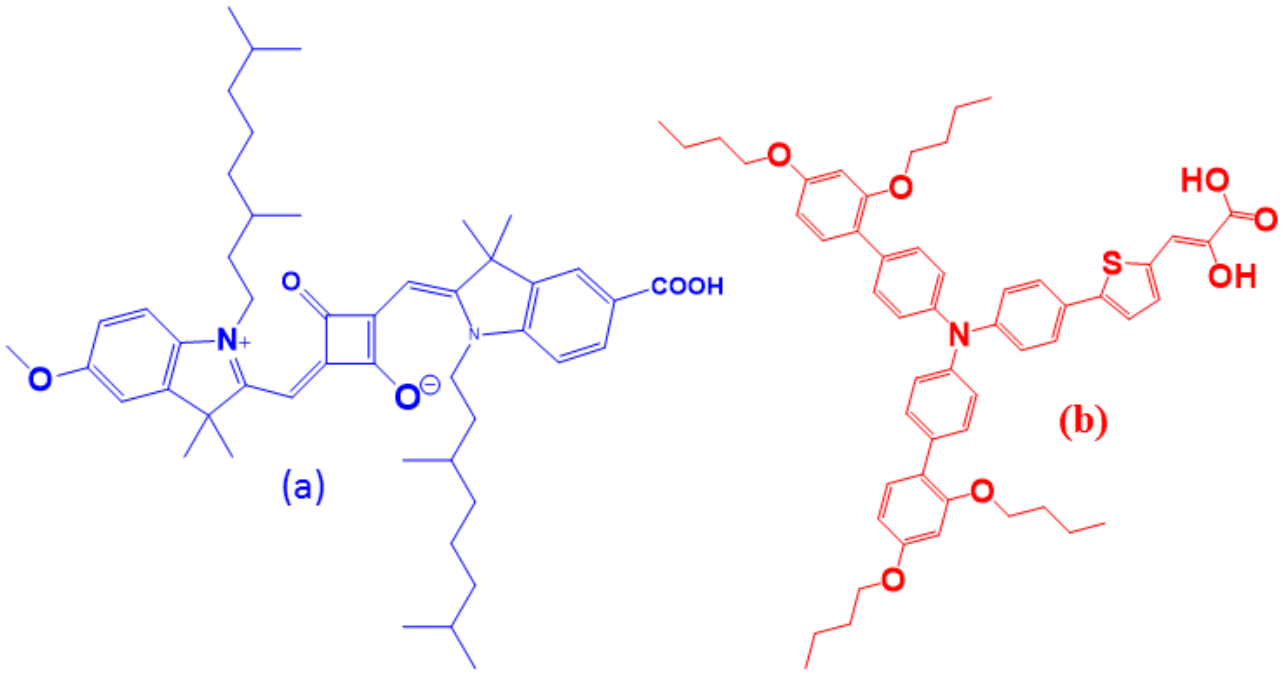

Figure-1

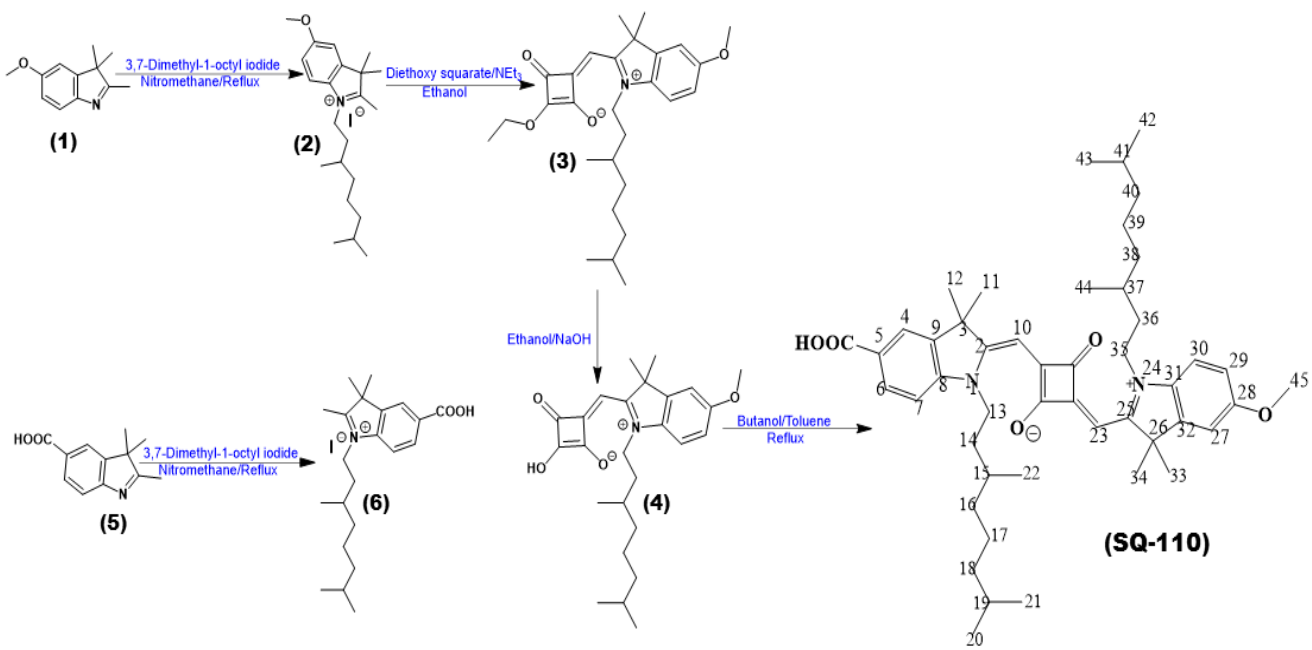

Figure-2

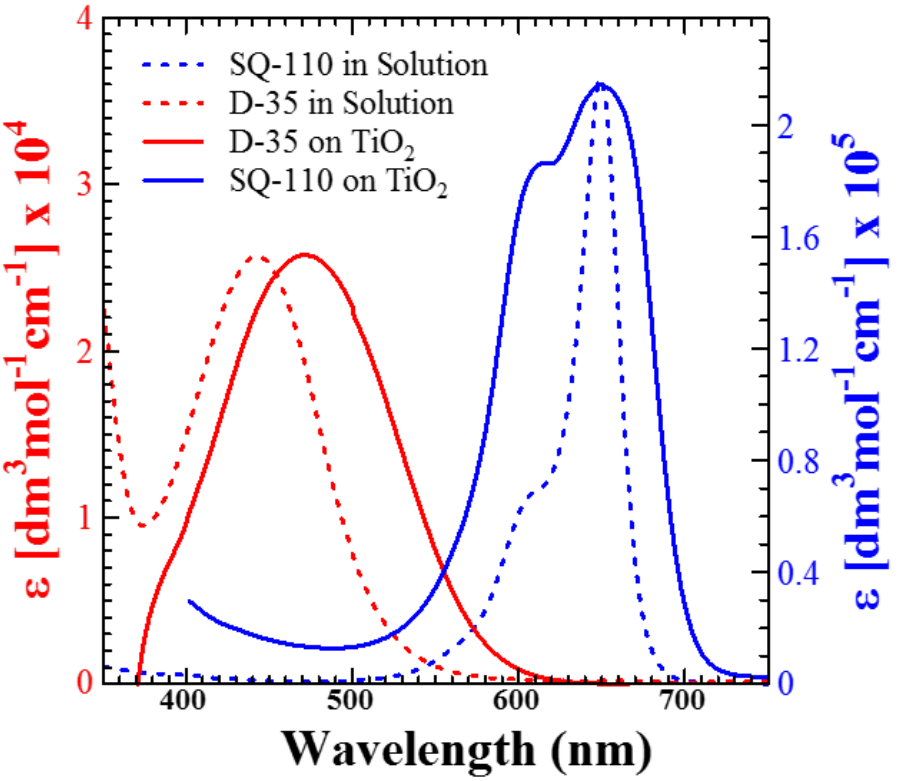

Figure-3

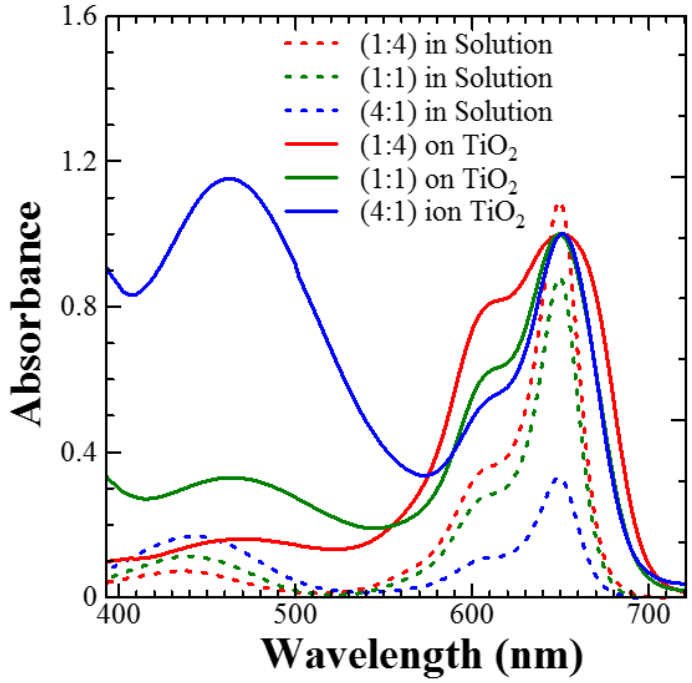

Figure-4

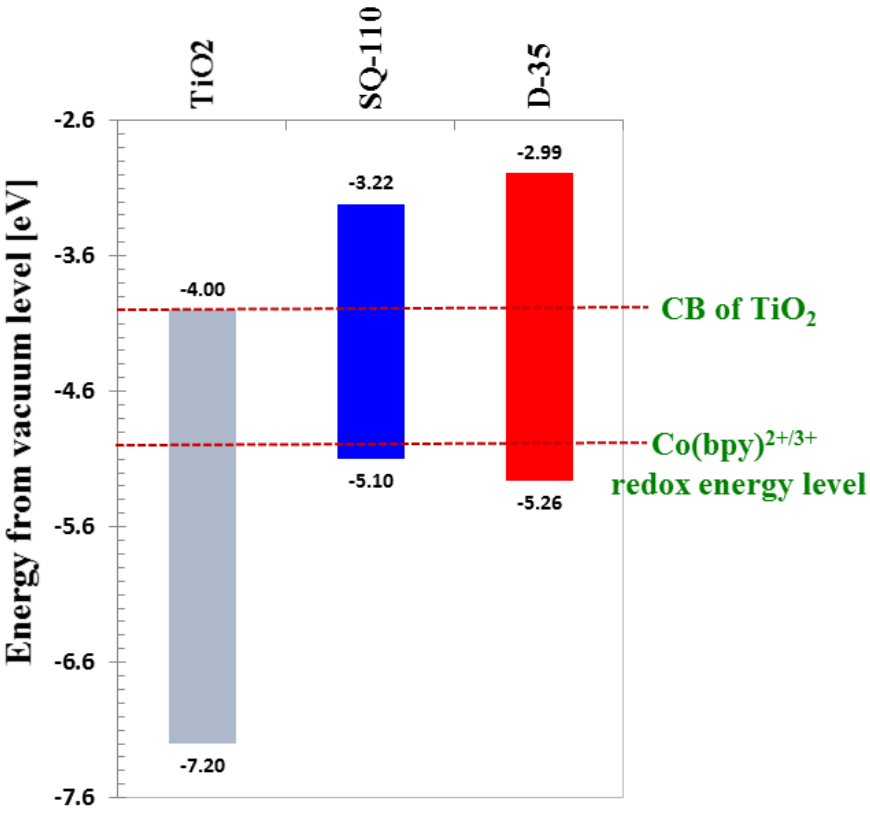

Figure-5

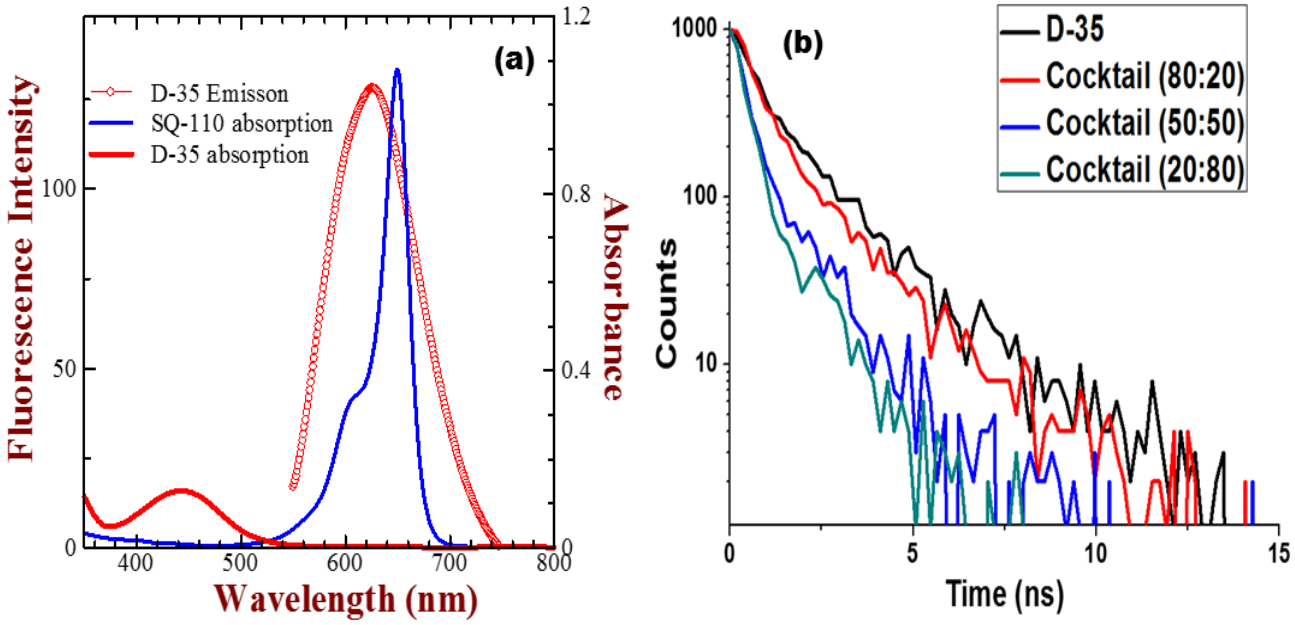

Figure-6

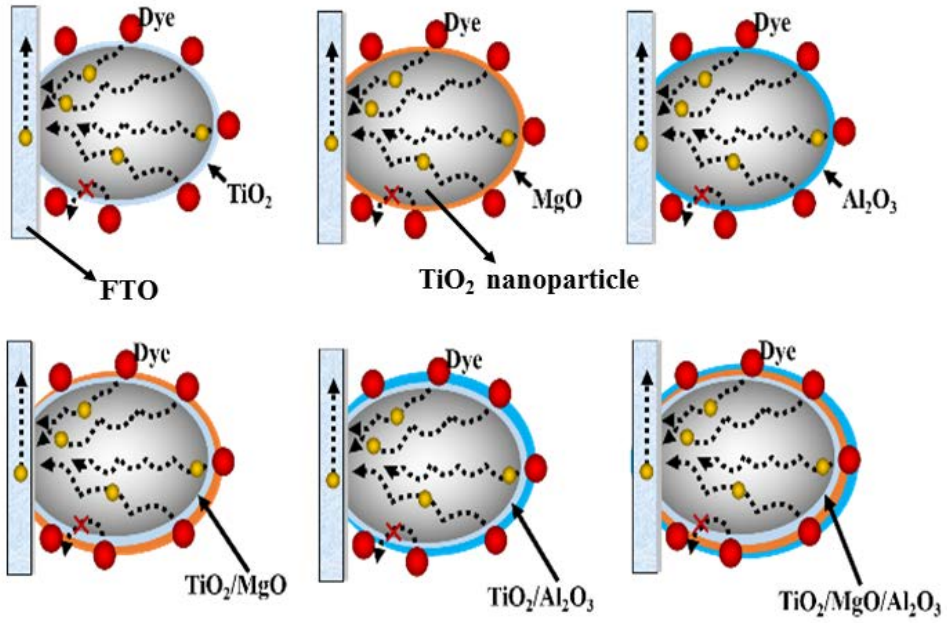

Figure-7

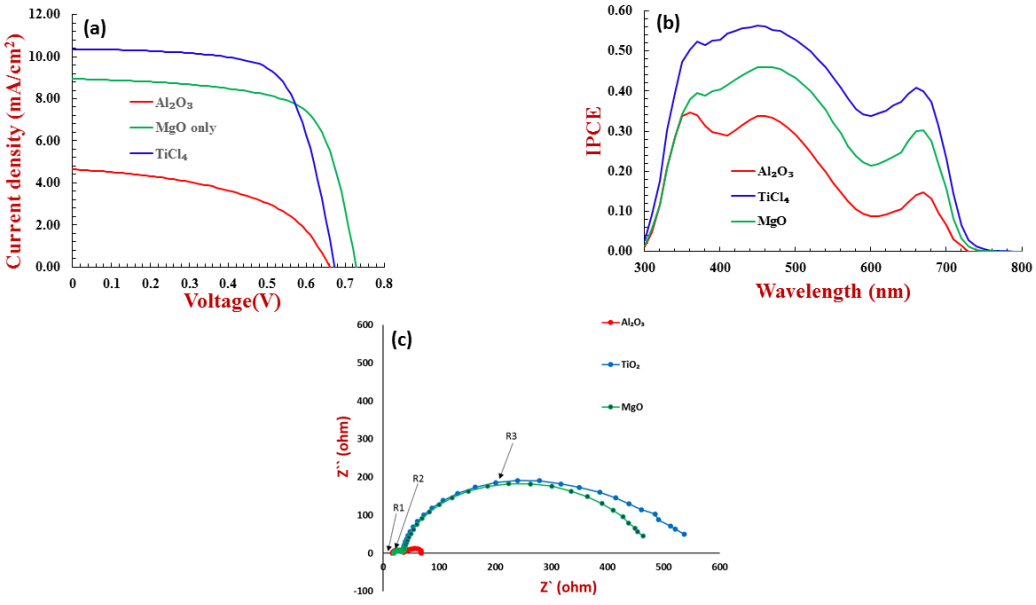

Figure-8

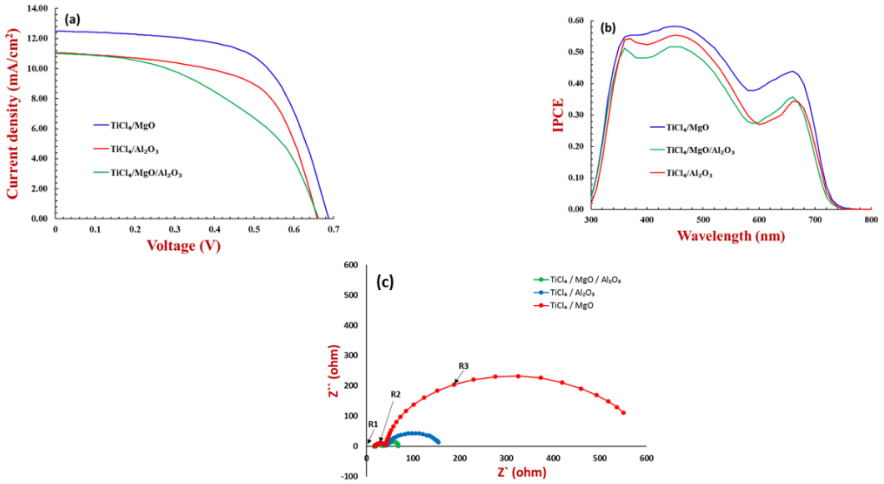

Figure-9

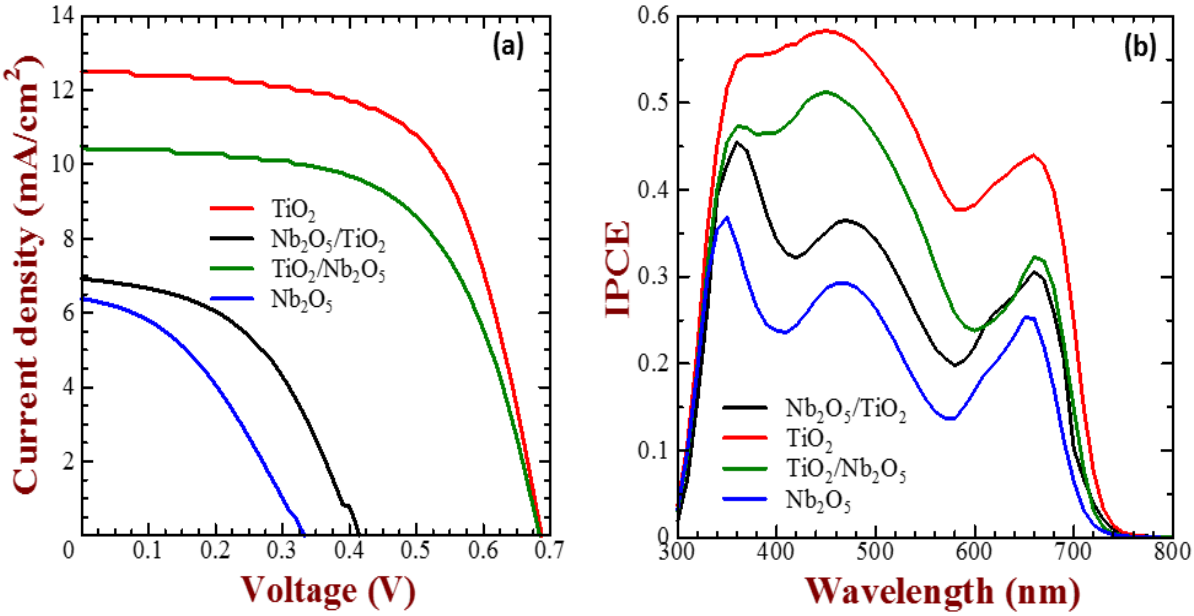

Figure-10

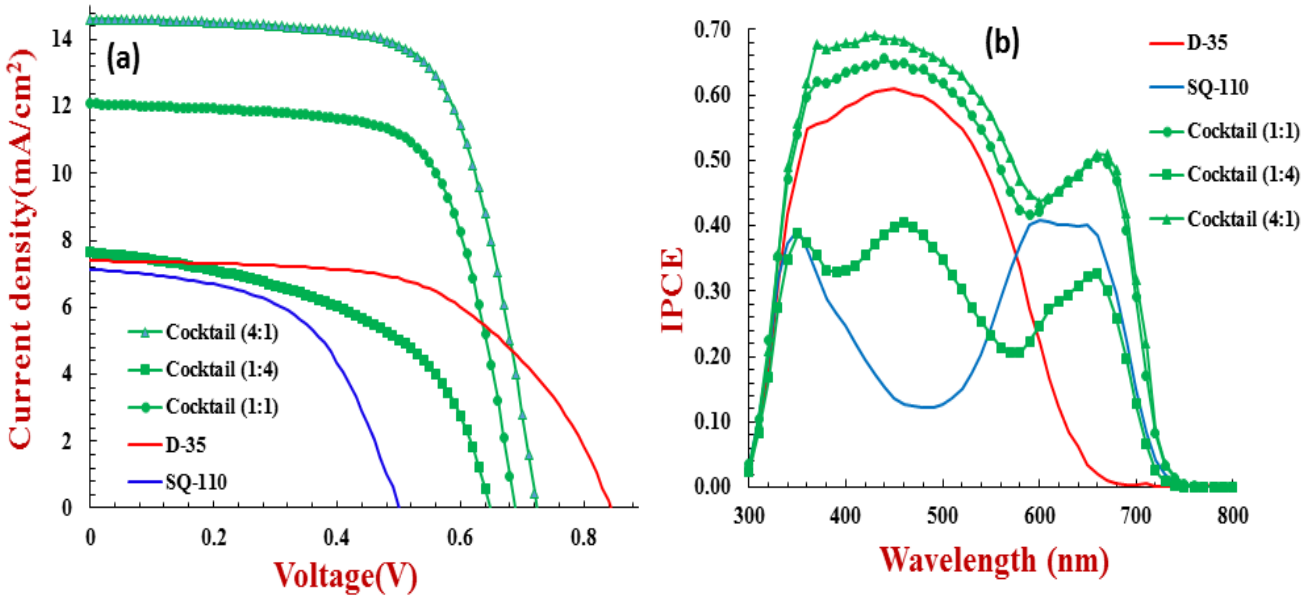
(a)
Current density(mA/cm²)
Voltage(V)
Cocktail (4:1)
Cocktail (1:4)
Cocktail (1:1)
D-35
SQ-110
(b)
IPCE
Wavelength (nm)
D-35
SQ-110
Cocktail (1:1)
Cocktail (1:4)
Cocktail (4:1)

Figure-11